Nano Today 42 (2022) 101347

Contents lists available at ScienceDirect

Nano Today

journal homepage: www.elsevier.com/locate/nanotoday

Area-selective and precise assembly of metal organic framework particles by atomic layer deposition induction and its application for ultra-sensitive dopamine sensor

Zhe Zhao[a,b], Ye Kong[a,b], Gaoshan Huang[a,b,d,*], Chang Liu[a,b], Chunyu You[a,b], Zhijia Xiao[a,b], Hongqin Zhu[a,b,e], Ji Tan[e], Borui Xu[a,c,d], Jizhai Cui[a,b,d], Xuanyong Liu[e], Yongfeng Mei[a,b,c,d,*]

[a] Department of Materials Science, Fudan University, Shanghai 200433, PR China
[b] International Institute for Intelligent Nanorobots and Nanosystems, Fudan University, Shanghai 200438, PR China
[c] Shanghai Frontiers Science Research Base of Intelligent Optoelectronics and Perception, Institute of Optoelectronics, Fudan University, Shanghai 200438, PR China
[d] Yiwu Research Institute of Fudan University, Yiwu 322000 Zhejiang, PR China
[e] State Key Laboratory of High Performance Ceramics and Superfine Microstructure, Shanghai Institute of Ceramics, Chinese Academy of Sciences, Shanghai 200050, PR China

ARTICLE INFO

Article history:
Received 25 August 2021
Received in revised form 7 November 2021
Accepted 17 November 2021
Available online 25 November 2021

Keywords:
Atomic layer deposition
PCN-333 film
Area-selective assembly
Dopamine sensor

ABSTRACT

Weak interactions, non-uniformity and powdery assemblies limit the wide application of metal organic framework (MOF) in devices. Here we report a new strategy for area-selective assembly of MOF particles to prepare a thin film with the assistance of atomic layer deposition (ALD). Self-assembled hierarchically porous Fe-based MOF (PCN-333) films were formed on both flat and complex three-dimensional (3D) substrates by combining gas and liquid fabrication approaches, and can be precisely patterned with photolithography. We demonstrate that the PCN-333 film obtained possesses excellent electrochemical activity and can be applied in dopamine sensing for ultra-high sensitivity of 4637.78 μA mM^{-1} cm^{-2} with a wide linear range and a low limit of detection. Moreover, the PCN-333 film composite achieves a function of good selectivity of distinguishing dopamine and ascorbic acid. This strategy is promising to prepare MOF film-based on-chip devices with advanced functions.

Introduction

The synthesis and development of nanoparticles have captivated researchers for decades [1,2]. Among all the nanoparticles, metal organic framework (MOF) particles have attracted tremendous attention due to their large surface area, controllable structure, and unsaturated metal coordination sites [3]. In order to further utilize MOF in particle state as active layer for more advanced applications in devices, the assembly of MOF nanoparticles has been pursued for the applications in sensors [4], energy storage devices [5], and catalysts [6]. These efforts have sought to obtain MOF particle materials with desired arrangement, often through the integration of MOFs on substrates [7,8]. However, some apparent drawbacks such as poor adhesion, non-uniformity, and severe aggregations exist among these strategies [7,9]. Precise manipulation of MOF particles is still challenging. Some pioneer researchers used oxides as start materials to guide the assembly of MOF particles [10,11], but the types of prepared MOFs is limited.

Inspired by previous atomic layer deposition (ALD)/molecular layer deposition (MLD)-prepared MOF structures [12,13], here we present a universe strategy that combines the gas phase (i.e., ALD) with liquid phase to prepare high-quality MOF film on complex substrate, where ALD-oxide nanomembrane was used to induce the assembly of MOF particles into uniform film. By this means, we have successfully prepared ZIF-67 [14–16], ZIF-8 [17], and Ni-MOF (Ni) [18] films on various substrates, and the composite structure has a wide range of advantageous applications such as catalysts, supercapacitors, and sensors [14,16,17]. However, up to now the

Abbreviations: MOF, metal organic framework; ALD, atomic layer deposition; 3D, three-dimensional; MLD, molecular layer deposition; DA, dopamine; LOD, limit of detection; HDS, hydroxyl double salt; XRD, X-ray diffraction; H_3TATB, 4,4',4''-s-Triazine-2,4,6-triyl-tribenzoic acid; SEM, scanning electron microscopy; EDS, energy dispersive spectrometer; XPS, X-ray photoelectron spectroscopy; PBS, phosphate buffer solution; CA, citric acid; THAM, tromethamine; LA, lactic acid; GL, glucose; RSD, relative standard deviation; DMF, N, N-dimethylformamide; DEZ, Diethylzinc; BET, Brunauer-Emmett-Teller; BJH, Barrett Joyner Halenda; GC, glass carbon

* Corresponding authors at: Department of Materials Science, Fudan University, Shanghai 200433, PR China.
E-mail addresses: gshuang@fudan.edu.cn (G. Huang), yfm@fudan.edu.cn (Y. Mei).

https://doi.org/10.1016/j.nantod.2021.101347
1748-0132/

application of MOFs in an on-chip device is still scarce due to their inconvenient integration on substrates. The area-selective and precise assembly of MOF is still a challenge, and the versatility of MOF materials also needs to be expanded.

Herein, we utilized ZnO nanomembrane prepared by ALD as an induction layer to prepare PCN-333 (Fe) film consisting of MOF particles. We demonstrated that the current approach can not only assemble patterned MOF film on a flat substrate with the help of photolithography but also produce the MOF layer on complex three-dimensional (3D) frameworks forming a hierarchical composite structure. The obtained PCN-333 (Fe) film exhibited outstanding electrochemical activity due to ordered assembly of particles and firm attaching on the substrate, which can be applied in non-enzyme sensing of dopamine (DA). The fabricated sensor demonstrates an ultra-high sensitivity of 4637.78 μA mM^{-1} cm^{-2} with a low limit of detection (LOD) of 0.14 μM. We believe that the precise assembly of MOF particles can open a new window for MOF-related structures and can be applied in MOF film-based integratable devices for various advantageous applications.

Results and discussion

Fig. 1a–c shows the schematic and SEM images of the assembly process of PCN-333 film on Si wafer by induction effect of ALD-ZnO nanomembrane. Due to the uniform deposition of ALD, a dense and conformal ZnO membrane was firstly deposited on the surface of the wafer [19]. No morphological change before and after ALD can be seen from Fig. 1a, indicating a dense and uniform nanomembrane prepared by ALD. According to our previous investigation [15], the thickness of ALD-ZnO nanomembrane is ~50 nm, and the multi-crystal ZnO nanomembrane formed at 150 °C. We believe this ZnO nanomembrane can provide vast nucleation sites for the following assembly of MOF particles. After Fe(III) was added, a large amount of 2D nanosheets appeared on the surface of Si substrate (Fig. 1b). This process is considered to be the key issue in the preparation of the target MOF film, where ALD-ZnO nanomembrane gradually reacted with Fe(III) ion. Similar to our previous investigations [14,16], it is highly possible that Zn(II) ions and Fe(III) ions formed Zn, Fe hydroxyl double salt (Zn, Fe-HDS), and corresponding X-ray diffraction (XRD) pattern of this intermediate is shown in Fig. S1. Sharp peaks emerge, which is different from $FeCl_3{\cdot}6H_2O$ and ALD-ZnO, indicating the formation of a new phase. After that, when the organic components (4,4′,4′′-s-Triazine-2,4,6-triyl-tribenzoic acid, H_3TATB) were added, the lamellar sheets began to collapse and release Fe(III), which coordinated with H_3TATB continuously, and the produced MOF particles were assembled into a dense film (Fig. 1c). The cross-sectional scanning electron microscopy (SEM) image of PCN-333 film is shown in Fig. S2, and a uniform PCN-333 film with a thickness of ~5 μm can be seen. The corresponding energy dispersive spectrometer (EDS) mapping results are shown in Fig. S3, demonstrating that Fe, C, N, and O elements are evenly distributed in the film. We conclude that the whole assembly process might be based on the following two equations [20,21]:

$$ZnO+2FeCl_3{\cdot}6H_2O \rightarrow [(Zn, Fe_2)(OH)_2]\ Cl_6{\cdot}11H_2O \quad (1)$$

$$[(Zn, Fe_2)(OH)_2]\ Cl_6{\cdot}11H_2O+H_3TATB \rightarrow 2PCN\text{-}333\ (Fe)+Zn^{2+}+6Cl^{-}+4H^{+} \quad (2)$$

This strategy has three significant advantages for device fabrication. Firstly, all the assembly processes occur on the surface of substrate, which makes it possible to selectively assemble MOF film at a certain area. Besides, taking advantage of ALD technique, the target PCN-333 layer is attached firmly to substrates, suggesting MOF film can conformally and uniformly wrap on the surface of even complex 3D substrates. Thirdly, the precise assembly inhibits the aggregation of MOF particles. For comparison, we also grew PCN-333 film onto the wafer without ALD-ZnO nanomembrane. As shown in Figs. S4 and S5, without ALD-ZnO nanomembrane as an induction layer, severe aggregation of particles with different sizes and big cracks can be observed in the film, indicating poor adhesion and non-uniformity of the film. By contrast, after the current induction process is engaged, the PCN-333 film is uniform and smooth (Fig. 1c). We also prepared PCN-333 powders in solution for comparison. XRD patterns of both PCN-333 film and powder in Fig. 1d show sharp peaks in accordance with the previous reports [22,23], confirming the successful formation of PCN-333 film. In addition, SEM image of PCN-333 powder (Fig. S6) shows that they are regular octahedral shapes, which are slightly various from the structure in PCN-333 film. This phenomenon can be ascribed to the fact that during PCN-333 film formation on the substrate, the contact between particles and the substrate limited the crystal growth. In order to investigate the pore structure of PCN-333 film, the nitrogen adsorption-desorption isotherms experiment was carried out and corresponding pore size distributions of PCN-333 film on Si wafer and PCN-333 powder are shown in Fig. 1e and f and corresponding insets. The PCN-333 film and PCN-333 powder exhibit similar isotherms, and two steep increases at $P/P_0 = 0.3$ and 0.45 on the nitrogen adsorption isotherm correspond to two types of mesoporous structure of film [23]. In addition, it is worth noting that the specific surface area of film was contributed by MOF films because the Si wafer is non-porous. Due to the small thickness, the specific surface area of PCN-333 film is reduced to 105 m^2 g^{-1}. As shown in Fig. 1f, a hierarchically porous structure of PCN-333 film can be noted. An apparent micropore peak located at 1.47 nm and two mesopore peaks located at 2.89 and 3.81 nm are remarkable. The existence of micropores makes for the exposure of the active sites, while mesopores are beneficial to the penetration of electrolyte [3]. The pore structure of PCN-333 powder is similar to the film, proving that the complex pore structure with both micropore and mesopore can be preserved during the assembly process.

In order to further demonstrate the ability of precise assembly of MOF film, patterned PCN-333 film was realized. As shown in Fig. 1g, we firstly deposited ZnO nanomembrane on Si wafer as induction layer. Photoresist pattern on ZnO nanomembrane was prepared by using photolithography and then the exposed ZnO was etched away by HCl. Photoresist layer was washed with acetone in the next step and the patterned ZnO nanomembrane was used in the assembly process to form patterned PCN-333 film. The SEM image with corresponding EDS mapping of patterned PCN-333 film is shown in Fig. 1h. C element uniformly dispersed on six-pointed star pattern, which originates from the organic linker of PCN-333. While the film coating makes the distribution of Si content is opposite to that of C content. In addition, we should stress that this are-selective and precise assembly strategy via photolithography of oxide nanomembrane can be expanded to other MOF film (Fig. S7). Thus, the strategy is capable of producing more complex geometries and should be promising in preparing micro-/nano-devices for more advanced functions.

As mentioned above, the advantage of conformality during ALD makes the current approach feasible in assembling MOF film on substrate with 3D geometry. In this work, we prepared conformal PCN-333 film on the complex 3D framework for advanced electrochemical application. Here we chose Ni foam with 3D interconnective network as substrate. Common methods to integrate MOFs on 3D substrates have some considerable drawbacks, such as non-uniformity, poor attachments, and severe aggregation [7,8], which hinder the improvement of electrochemical properties. Fig. S8 shows PCN-333 particles directly grown on Ni foam without ALD pre-treatment. A few PCN-333 particles can be observed and aggregations of the particles in the gap are noticeable. We then prepared PCN-333 film on Ni foam by using ALD-ZnO nanomembrane as an induction layer. As shown in Fig. 2a and b, bare Ni foam displays a

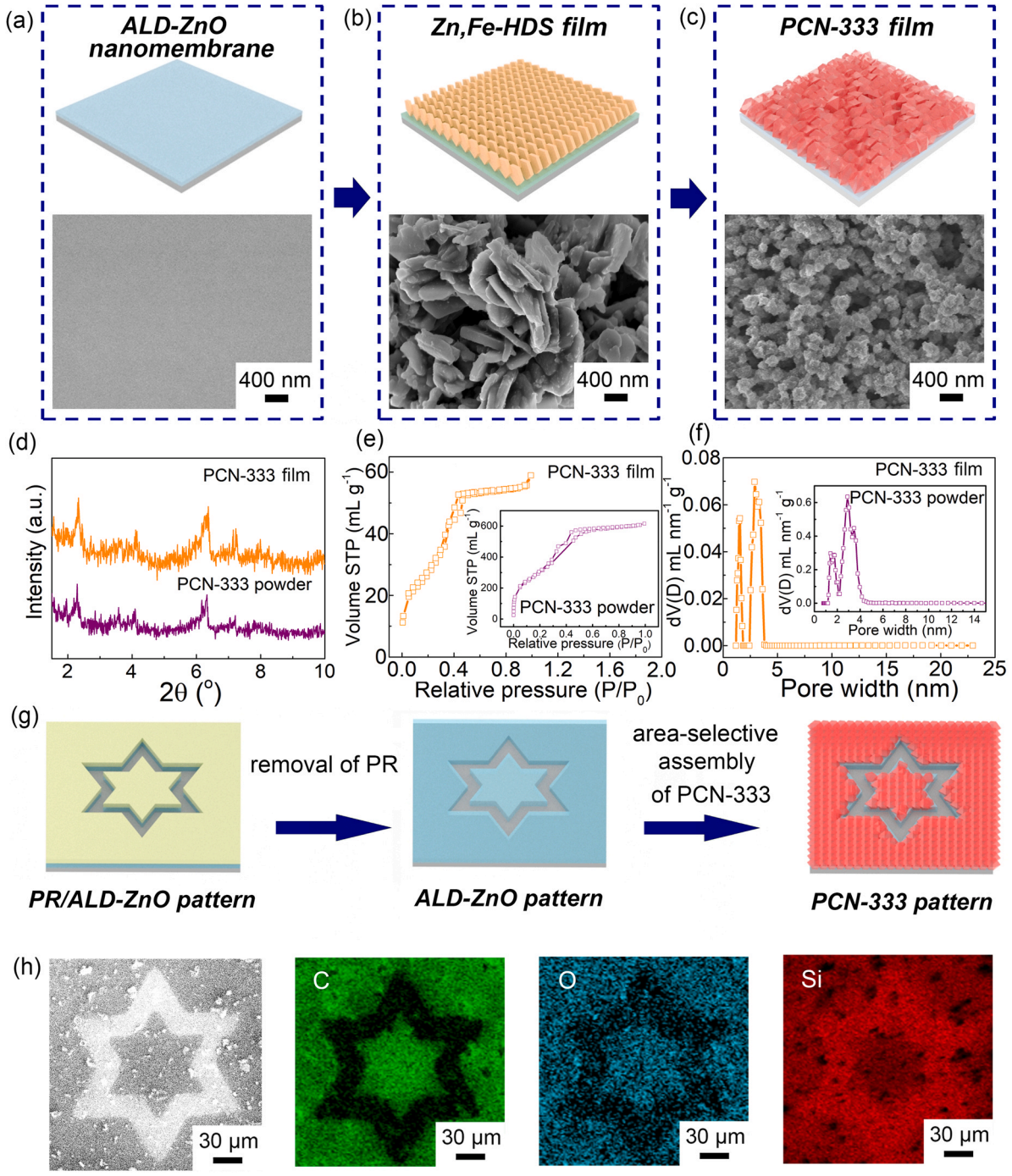

Fig. 1. Fabrication and characterization of PCN-333 film on flat substrate. (a)-(c) Schematic of the preparation process and corresponding SEM images. ALD-ZnO nanomembrane, Zn, Fe-HDS film, and PCN-333 film are specifically demonstrated. (d) XRD patterns of PCN-333 film and PCN-333 powder. (e) and (f) Nitrogen adsorption-desorption isotherms and corresponding pore size distributions of PCN-333 film. The corresponding insets show the results from PCN-333 powder. (g) Schematic of the preparation process of patterned PCN-333 film. (h) SEM image and EDS mappings of patterned PCN-333 film.

3D frameworks structure with a smooth surface. When pre-treated with ZnO nanomembrane of 300 ALD cycles, no obvious morphology changes can be observed (Fig. 2c and d). After assembly of MOF film, a high mass loading of PCN-333 film attached to the surface of skeleton of Ni foam can be observed (Fig. 2e and f), which is distinguished from direct growth (Fig. S8). The enlarged SEM image of PCN-333 film is shown in the inset of Fig. 2f, and PCN-333 particles with good crystal morphology can be seen. SEM image with EDS mapping of PCN-333 film on Ni foam is shown in Figs. 2g and S9. Homogeneous distribution of a large amount of Fe and C implies the successful assembly of uniform MOF film. The small amount of Zn should originate from the induction layer. XRD pattern of PCN-333 film on Ni foam is shown in Fig. 2h. Sharp peaks located at 35–65° belong to the Ni substrate, while peaks at small angles from 2 to 10° match well to the PCN-333 structure. The XRD results further confirm the successful growth of target MOF on 3D substrate. In addition, the elemental composition and chemical states of PCN-333 film are investigated by X-ray photoelectron spectroscopy (XPS), and the results confirm the presence of Fe, O, and C (Fig. 2i and j). The high-resolution Fe 2p spectrum can be deconvoluted into 3 peaks at 725.3,

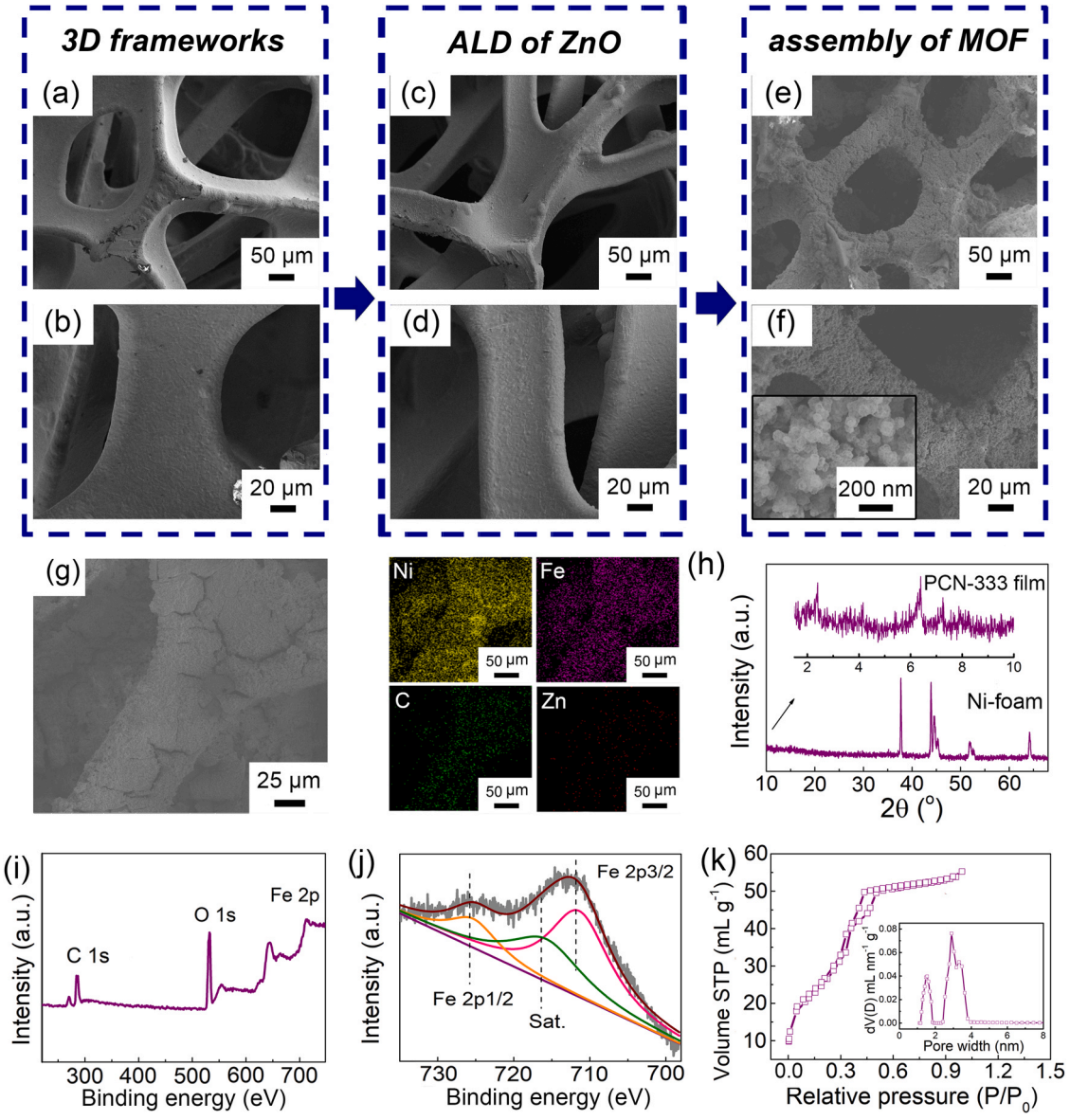

Fig. 2. Fabrication and characterization of PCN-333 film on 3D substrate. SEM images of (a) and (b) bare Ni foam, (c) and (d) ALD-ZnO nanomembrane-coated Ni foam, and (e) and (f) PCN-333 film on Ni foam with low and high magnifications. (g) SEM image and corresponding EDS mappings of PCN-333 film on Ni foam. (h) XRD pattern of PCN-333 film on Ni foam. (i) XPS survey scan of PCN-333 film on Ni foam. (j) Corresponding high-resolution Fe 2p XPS spectrum. (k) Nitrogen adsorption-desorption isotherm and corresponding pore size distribution (inset).

711.4, and 715.7 eV, respectively corresponding to the Fe 2p1/2, Fe 2p3/2, and satellite species [24]. The XPS curves of PCN-333 film disclose the existence of Fe (III), which provides high oxidation activity to achieve high-performance electrochemical application [25]. The nitrogen adsorption-desorption isotherms and corresponding pore size distributions of PCN-333 film on Ni foam are shown in Fig. 2k and its inset. The pore structure of this composite is almost identical to the PCN-333 film on a flat Si wafer with a surface area of 102 m^2 g^{-1}. A micropore with an average pore width of 1.54, 2.89, and 3.31 nm can be observed (inset of Fig. 2k), indicating a hierarchically porous structure. Due to the negligible surface area of bare Ni foam, the large surface area of the composite suggests that the composite possesses a very high mass loading of PCN-333.

To further investigate the electrochemical activity of the PCN-333 film on Ni foam quantitatively, the active area of the composites is studied by using $K_3[Fe(CN)_6]$ as the probe. As shown in Fig. 3a and c, a pair of oxidation and reduction peaks can be observed in the CV scans of different electrode materials (i.e., composite and bare Ni foam), and the oxidation and reduction peak currents increase as the scan rate increases from 30 to 120 mV s^{-1}. The active area (S) of electrode materials can be calculated by the Randles-Sevcik equation: $I_{peak} = (2.69 \times 10^5)n^{3/2}SD^{1/2}Cv^{1/2}$, where n is the number of transferred electrons, D is the diffusion coefficient of $K_3[Fe(CN)_6]$, and C is the bulk concentration of $K_3[Fe(CN)_6]$ [26]. Herein, the values of S were evaluated to be 0.092 and 0.04 cm^2 for the composites and bare Ni foam, respectively, based on the slope of the peak current versus the square root of the scan rate (Fig. 3b and d). It is clear that the composite exhibits more than twice of active area compared with Ni foam. This may be ascribed to the high surface area and high active sites exposure of MOF film, which is conducive to the contact of active species in electrolyte and interfacial electron transfer, thereby further enhancing the electrochemical performance.

The sensing property of PCN-333 composite is firstly investigated by CV scanning. As shown in Fig. S10, no peak can be seen for electrode in pure phosphate buffer solution (PBS), which is consistent with the fact that no electrochemical reaction takes place on

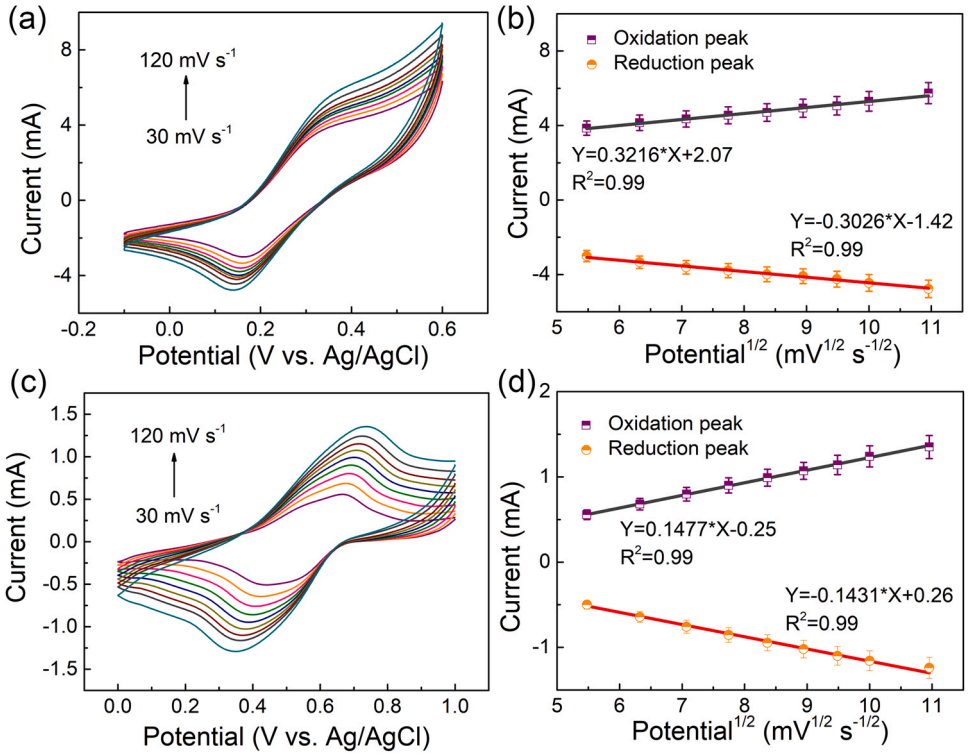

Fig. 3. Electrochemical activity of PCN-333 composite. CV scans at various scan rates of 30–120 mV s^{-1} in 0.1 M PBS (PH = 7.2) containing 5 mM $K_3[Fe(CN)_6]$of (a) PCN-333 film on Ni foam and (c) bare Ni foam. (b) and (d) oxidation peak current and reduction peak current as functions of square root of the scan rate, derived respectively from (a) and (c). Error bars represent the standard deviations of three measurements.

the electrode. Upon addition of 1 mM DA, apparent oxidation and reduction peaks associated with the oxidation and reduction of DA and Fe ion appears, indicating a high electrochemical activity of PCN-333 film toward oxidation of DA. To further confirm the sensing performance of the PCN-333 film quantitatively, we applied this PCN-333 film as a highly sensitive DA electrochemical sensor, and current-time (I-t) measurement was used to evaluate the electrochemical sensing performance. In order to identify the appropriate potential for DA sensing, Fig. S11 shows the influence of applied potential on the amperometric response of 1 mM DA. Obviously, at 0.4 V, the composite exhibits a remarkable and stable response. The mechanism of DA sensing of the PCN-333 film could be attributed to the following equations:

$$\text{PCN-333-Fe(III)}-2e^{-}+C_8H_9N(OH)_2 \rightarrow \text{PCN-333-Fe(II)}+C_8H_9NO_2+2H^{+} \quad (3)$$

$$\text{PCN-333-Fe(II)} \rightarrow \text{PCN-333-Fe(III)} \quad (4)$$

In the present work, the non-enzymatic DA sensing performance of the composite is quantitatively evaluated at 0.4 V. Fig. 4a illustrates the I-t curve of the sensor with the successive addition of DA in 0.1 M PBS at a potential of 0.4 V. With the addition of DA, apparent and rapid current responses can be seen, indicating a real-time sensing ability. The corresponding calibration plot related to the concentration is shown in Fig. 4b. According to the calibration plot, the composite exhibits an ultrahigh sensitivity of 4637.78 μA mM^{-1} cm^{-2} with a linear range of 0.5–140 μM (linear regression equation: Y = 0.02087X-0.00501; correlation coefficient (R^2 = 0.98)). In addition, the LOD is calculated by using the equation: LOD = 3σ/S, where σ is the standard deviation and S is the sensitivity, and thus a LOD of 0.14 μM is obtained. We should stress that these values can compare favorably with those of plenty of other MOF-based electrochemical DA sensors in previous reports [27–34]. The detailed comparison of the sensing performance is summarized in Table 1. More, CV curve of PCN-333 film at a scan rate of 20 mV s^{-1} in 0.1 M PBS containing 1 mM DA compared with that of PCN-333 powder is shown in Fig. S12. The area surrounded by CV curve of PCN-333 film is much larger than that of PCN-333 powder, indicating a better electrochemical activity.

The anti-interference ability is also important for evaluating the sensing performance. Fig. 4c shows the I-t curve of PCN-333 film with the continuous addition of 1.5 mM DA, 0.1 mM KCl, 0.1 mM NaCl, 0.1 mM citric acid (CA), 0.1 mM tromethamine (THAM), 0.1 mM lactic acid (LA), and 0.1 mM glucose (GL), and the I-t curve demonstrates that interferents produce little current response compared with DA, proving the good anti-interference ability. In addition, selectivity is evaluated to verify the practicality of the sensor. As shown in Fig. S13, the I-t curve of the composite with consecutive introduction of 1 mM DA and 3 mM interferents (e.g., NaCl, KCl, LA, GL, and AA) illustrates the significant current response with the addition of target DA. Except for a tiny response of AA, one can see only negligible response when adding a series of interferents, illustrating good selectivity of PCN-333 film to the target molecule. It is worth noting that negligible current responses from interferents are observed when the concentrations of interferents are three times higher than that of target DA, implying the great potential in practical applications. In biological tissues, electrochemical detection of DA is essentially prevented by the presence of high levels of AA, which results in a large over-potential for oxidation with conventional electrodes [35]. Thus, the distinguishing of DA and AA is important for electrochemical DA sensor. The PCN-333 film can also effectively achieve this function. As shown in Fig. S14, with the successive addition of 1 mM DA and 1 mM AA, the response of the PCN-333 film to DA was more than three times larger than that to AA, indicating a selective determination of DA. The electrochemical stability of PCN-333 film was further testes in 0.1 M NaOH containing 1 mM DA at 0.4 V. As shown in Fig. 4d, the composite exhibits a stable current response after 24 h. After that, with the addition of

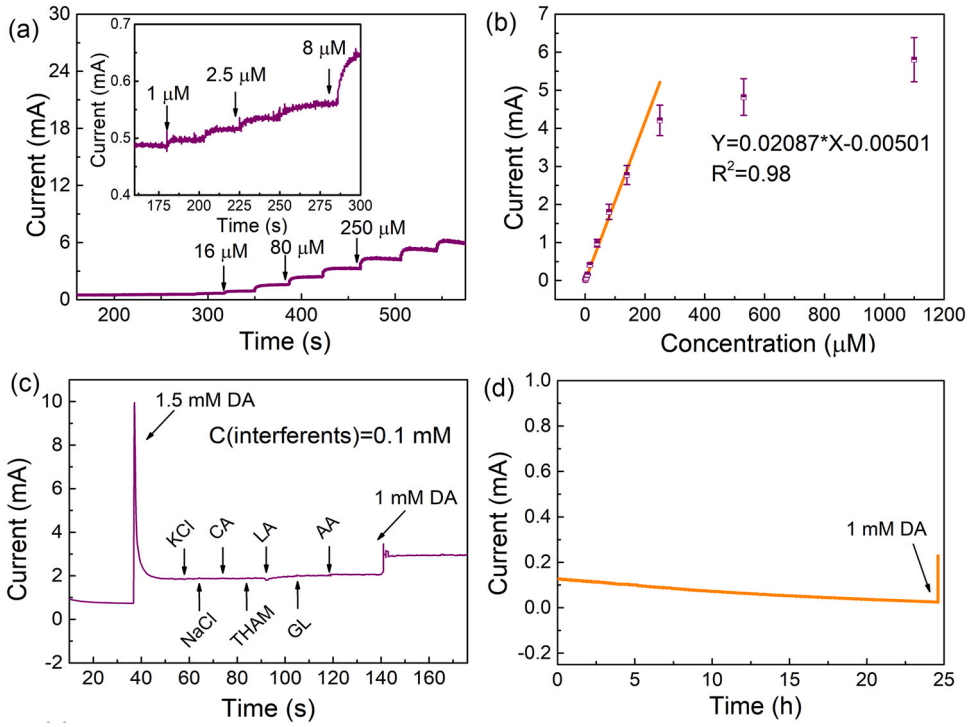

Fig. 4. Sensing performance of PCN-333 composite. (a) I-t curve of PCN-333 film on Ni foam with the successive addition of DA in 0.1 M PBS at a potential of 0.4 V. The inset shows the enlarged image. (b) Calibration plot derived from (a). (c) I-t curve of PCN-333 film on Ni foam for the continuous addition of 1.5 mM DA, 0.1 mM KCl, 0.1 mM NaCl, 0.1 mM CA, 0.1 mM THAM, 0.1 mM LA, 0.1 mM GL, 0.1 mM AA, and 1 mM DA at 0.4 V. (d) I-t curve of PCN-333 film on Ni foam in 0.1 M PBS with 1.0 mM DA at 0.4 V. 1 mM DA was added to the solution after 24 h to test the recovery performance.

Table 1
Summary of DA sensing performance of MOF-based structure reported in literature published in recent years.

Sample	Sensitivity μA mM^{-1} cm^{-2}	Linear range (μM)	LOD (μM)	Ref
ZIF-67/rGO	93.7	0.25–66.25	0.052	[27]
Fe_2Ni MIL-88B/GCE	124.7	1.2–1800	0.4	[28]
R-Co_3O_4@MOFDC	3711	0–20	0.925	[29]
MOF-525–PEDOT NT	428	2–270	0.04	[30]
HKUST-1	/	0.5–100	0.2	[31]
MOFs/ERGO	156	0.2–300	0.013	[32]
PXa/Au/Cu-TCPP/GCE	/	5.0–125	1.0	[33]
RGO/ZIF-8	1527	0.1–100	0.03	[34]
PCN-333 film	**4637.78**	**0.5–140**	**0.14**	**This work**

1 mM DA, the composite still exhibits an obvious current response due to the great recovery ability. In addition, the reproducibility of the sensor is evaluated by sensing 1 mM DA by using the same sensor for 6 times. As shown in Fig. S15, the overlap of the I-t curves indicates the identical response, and the relative standard deviation (RSD) was 4% (inset of Fig. S15), proving the good reproducibility of the sensor. We consider that the outstanding sensing property of the PCN-333 film can be attributed to its unique structural properties. First, continuous MOF film on 3D substrate provides a conductive pathway for ion transfer. Second, assembly of Fe-based MOF guarantees uniform dispersion of active sites in the whole skeleton, leading to maximized possible activity. Furthermore, the large surface area of PCN-333 film makes the target molecules easy to access the catalytic sites. Also, the mesopores of PCN-333 film enhance the capture of target molecules and penetration of electrolyte, thereby improving the sensing performance [36].

Conclusion

The PCN-333 film was fabricated on both 2D and 3D substrates with the assistance of ALD and can be patterned by photolithography. During growth, the PCN-333 particles was found to be precisely assembled from Zn, Fe-HDS, which is derived from ALD-prepared ZnO nanomembrane. A combination of gas and liquid fabrication approaches renders a dense and conformal MOF film attached to the substrate, and the film exhibits abundant hierarchically porous structure with a large surface area of 105 m^2 g^{-1}, leading to high electrochemical performance. In the case of DA sensing, PCN-333 film on Ni foam shows ultra-high sensitivity of 4637.78 μA mM^{-1} cm^{-2} with a wide linear range from 0.5 to 140 μM and a low LOD of 0.14 μM. We believe this strategy can provide a new route to prepare MOF film-based on-chip device, and more MOFs with versatile functions can be integrated into a multi-functional smart system.

Experimental section

Materials

Iron(III) chloride ($FeCl_3$) was purchased from Aladdin Ltd. (Shanghai, China). 4,4′,4′′-s-Triazine-2,4,6-triyl-tribenzoic acid (H_3TATB, 95%) was purchased from Sigma-Aldrich. D(+)-GL monohydrate (AR, ≥99.7%), LA (AR, ≥99.7%), N, N-dimethylformamide

(DMF), trifluoroacetic acid (AR, ≥99.7%), and potassium ferricyanide ($K_3[Fe(CN)_6]$) were obtained from Sinopharm Chemicals. DA hydrochloride (≥97%) and ascorbic acid (≥99.99%) were purchased from Aladdin Ltd. (Shanghai, China). The solution used for the electrochemical activity measurements was 0.1 M of PBS, pH 7.2 unless otherwise noted. All the reagents were used as received without further purification. The DI water used throughout all experiments was purified through a Millipore system.

ZnO nanomembrane deposited by ALD

ZnO nanomembrane was deposited on Ni-foam and Si-wafer through ALD technology reported in our previous study [16]. The deposition of ZnO nanomembrane was performed at 150 °C in a homemade reactor. Diethylzinc (DEZ) and DI water were used as precursors. A typical ALD cycle included DEZ pulse (50 ms), waiting time (5 s), N_2 purge (30 s), DI water pulse (30 ms), waiting time (5 s), and N_2 purge (30 s). In the current study, ZnO nanomembrane with 300 ALD cycles was deposited on substrates.

Fabrication of PCN-333(Fe) film on substrates

$FeCl_3$ (0.3 g) was dissolved in the DMF (50 mL) to form solution A. H_3TATB (0.25 g) was dissolved in the DMF (50 mL) to form solution B. ALD ZnO-coated substrates (substrates pretreated with 300 cycles ALD ZnO) was then placed into a beaker containing solution A. The beaker was sealed at 120 °C for 24 h. After cooling to room temperature (formation of HDS), solution B was added, and the mixture was sealed at 90 °C for another 24 h. After that, the substrates were taken out and washed with fresh DMF. The sample was subsequently dried in vacuum at 120 °C for 12 h. This process led to the formation of a uniform PCN-333 (Fe) film on the surface of substrates. In order to investigate the growth mechanism of the PCN-333 (Fe) film, reference samples were prepared with different aging time, and characterized with SEM.

Preparation of ZnO patterns

The patterns in the current work was based on a silicon substrate from the cut and cleaned silicon wafer. A uniform ARP-3510 photoresist (All resist GmbH) layer with a thickness of ~2 μm was firstly spin-coated on the silicon substrate. The photoresist layer was then patterned to arrays of certain shape by ultraviolet lithography (SUSS MA6). The exposed ZnO nanomembrane was etched away by dilute HCl. Photoresist layer was washed by acetone in the next step and the patterned ZnO nanomembrane was used in the assembly process to form patterned MOF film.

Synthesis of the PCN-333(Fe) powder

PCN-333 (Fe) powder was also synthesized for comparison. H_3TATB (0.25 g) and $FeCl_3$ (0.3 g) were dissolved in 100 mL DMF. The mixture was heated at 120 °C in an oven for 24 h until a brown precipitate formed. The product was centrifuged, washed with DMF for 3 times, and finally dried at 60 °C for 12 h in vacuum.

Structural characterizations

The morphologies of all the products were measured by a VEGA TS 5136 MM field-emission SEM (TESCAN Co., Czech). XRD patterns were measured by an X′Pert Pro X-ray diffractometer equipped with Cu Kα radiation (λ = 0.1542 nm) at a current of 40 mA and voltage of 40 kV. A Quadrasorb adsorption instrument (Quantachrome Instruments) was used to perform the nitrogen sorption/desorption measurements. The specific surface area was calculated using single-point Brunauer-Emmett-Teller (BET) method. The pore size distributions were calculated from nitrogen sorption data using Barrett Joyner Halenda (BJH) method provided by Quantachrome data reduction software ASiQwin Version 4.01. The EDS (Oxford X-Max 80T) was utilized to analyze the composition of the sample. XPS analyses were made with a VG ESCALAB 220I-XL device. The curve fitting of all XPS spectra was accomplished by using XPS Peak 4.1 software.

Electrochemical characterizations

The electrochemical DA sensing tests were evaluated on a CHI 660E (Chenhua Instrument, Shanghai, China) with three-electrode configuration. In our experiment, an Ag/AgCl (in saturated KCl solution) was used as the reference electrode and a graphite rod was used as the counter electrode. PCN-333 (Fe) film on Ni-foam was directly used as the working electrode. For the preparation of the working electrode, the PCN-333 (Fe) film on Ni-foam was tailored into a rectangle with the area of 10 × 20 mm^2. PCN-333 (Fe) powder modified glassy carbon (GC, diameter: 3 mm) was also used as the working electrode for comparison. Bare GC was firstly polished to a mirror successively using 1.0, 0.3 and 0.05 μm alumina slurry, and then sonicated alternately in ethanol and deionized water several times. The active materials ink was prepared by sonicating the mixture of 4.0 mg catalyst, 970 μL ethanol, and 30 μL Nafion (5 wt%) for 40 min. Next, 10 μL of the dispersion ink was dropped onto the well-polished GC electrode and then dried under ambient conditions.

CRediT authorship contribution statement

Zhe Zhao: Conceptualization, Methodology, Investigation, Data curation, Writing – original draft, Writing – review & editing. **Ye Kong:** Visualization, Data curation, Writing – review & editing. **Gaoshan Huang:** Conceptualization, Methodology, Investigation, Writing – review & editing, Supervision. **Chang Liu:** Writing – review & editing. **Chunyu You:** Writing – review & editing. **Zhijia Xiao:** Writing – review & editing. **Hongqin Zhu:** Writing – review & editing. **Ji Tan:** Writing – review & editing. **Borui Xu:** Writing – review & editing. **Jizhai Cui:** Writing – review & editing. **Xuanyong Liu:** Writing – review & editing. **Yongfeng Mei:** Supervision.

Declaration of Competing Interest

The authors declare that they have no known competing financial interests or personal relationships that could have appeared to influence the work reported in this paper.

Acknowledgments

This work was supported by the Natural Science Foundation of China (Nos. 51961145108 and 61975035), and the Science and Technology Commission of Shanghai Municipality (Nos. 19XD1400600, 20501130700, and 19JC1415500). Part of the experimental work had been carried out in Fudan Nanofabrication Laboratory and Jiangsu Ningbiao Science and Technology Co., Ltd.

Appendix A. Supporting information

Supplementary data associated with this article can be found in the online version at doi:10.1016/j.nantod.2021.101347.

References

[1] Y. Katayama, M. Kalaj, K.S. Barcus, S.M. Cohen, Self-assembly of metal-organic framework (MOF) nanoparticle monolayers and free-standing multilayers, J. Am. Chem. Soc. 141 (2019) 20000–20003.

[2] Q. Shi, W. Cheng, Free-standing 2D nanoassemblies, Adv. Funct. Mater. 30 (2020) 1902301.

[3] Z. Zhao, S.L. Liu, J.X. Zhu, J.S. Xu, L. Li, Z. Huang, C. Zhang, T.X. Liu, Hierarchical nanostructures of nitrogen-doped porous carbon polyhedrons confined in carbon nanosheets for high-performance supercapacitors, ACS Appl. Mater. Interfaces 10 (2018) 19871–19880.

[4] H.C. Sun, Y. Li, S.J. Yu, J.Q. Liu, Metal-organic frameworks (MOFs) for biopreservation: from biomacromolecules, living organisms to biological devices, Nano Today 35 (2020) 100985.

[5] L.P. Zhang, W. Wang, X.M. Ma, S.F. Lu, Y. Xiang, Crystal, interfacial and morphological control of electrode materials for nonaqueous potassium-ion batteries, Nano Today 37 (2021) 101074.

[6] W.S. Zhao, G.D. Li, Z.Y. Tang, Metal-organic frameworks as emerging platform for supporting isolated single-site catalysts, Nano Today 27 (2019) 178–197.

[7] H. Liu, H. Wang, T. Chu, M. Yu, Y. Yang, An electrodeposited lanthanide MOF thin film as a luminescent sensor for carbonate detection in aqueous solution, J. Mater. Chem. C 2 (2014) 8683–8690.

[8] W. Zhang, X. Yao, S. Zhou, X. Li, L. Li, Z. Yu, L. Gu, ZIF-8/ZIF-67-derived Co-N-x-embedded 1D porous carbon nanofibers with graphitic carbon-encased Co nanoparticles as an efficient bifunctional electrocatalyst, Small 14 (2018) 1800423.

[9] A. Centrone, Y. Yang, S. Speakman, L. Bromberg, G.C. Rutledge, T.A. Hatton, Growth of metal-organic frameworks on polymer surfaces, J. Am. Chem. Soc. 132 (2010) 15687–15691.

[10] K. Khaletskaya, S. Turner, M. Tu, S. Wannapaiboon, A. Schneemann, R. Meyer, A. Ludwig, G. Van Tendeloo, R.A. Fischer, Self-directed localization of ZIF-8 thin film formation by conversion of ZnO nanolayers, Adv. Funct. Mater. 24 (2014) 4804–4811.

[11] D. Zacher, O. Shekhah, C. Woell, R.A. Fischer, Thin films of metal-organic frameworks, Chem. Soc. Rev. 38 (2009) 1418–1429 38.

[12] E. Ahvenniemi, M. Karppinen, Atomic/molecular layer deposition: a direct gas-phase route to crystalline metal-organic framework thin films, Chem. Commun. 52 (2016) 1139–1142.

[13] K.B. Lausund, M.S. Olsen, P.-A. Hansen, H. Valen, O. Nilsen, MOF thin films with bi-aromatic linkers grown by molecular layer deposition, J. Mater. Chem. A 8 (2020) 2539–2548.

[14] Z. Zhao, Y. Kong, X.Y. Lin, C. Liu, J.R. Liu, Y.Y. He, L.L. Yang, G.S. Huang, Y.F. Mei, Oxide nanomembrane induced assembly of a functional smart fiber composite with nanoporosity for an ultra-sensitive flexible glucose sensor, J. Mater. Chem. A 8 (2020) 26119–26129.

[15] Z. Zhao, Y. Kong, C. Liu, G.S. Huang, Z.J. Xiao, H.Q. Zhu, Z.H. Bao, Y.F. Mei, Atomic layer deposition-assisted fabrication of 3D Co-doped carbon framework for sensitive enzyme-free lactic acid sensor, Chem. Eng. J. 417 (2021) 129285.

[16] Z. Zhao, Z.W. Zhang, Y.T. Zhao, J.R. Liu, C. Liu, Z.J. Wang, G.F. Zheng, G.S. Huang, Y.F. Mei, Atomic layer deposition inducing integration of Co, N codoped carbon sphere on 3D foam with hierarchically porous structures for flexible hydrogen producing device, Adv. Funct. Mater. 29 (2019) 1906365.

[17] Z. Zhao, Y. Kong, C. Liu, J.R. Liu, Z.J. Wang, G.F. Zheng, G.S. Huang, Y.F. Mei, Atomic layer deposition-induced integration of N-doped carbon particles on carbon foam for flexible supercapacitor, J. Mater. 6 (2020) 209–215.

[18] Z. Zhao, Y. Kong, G.S. Huang, C. Chen, W. Chen, Y.F. Mei, Nickel-based metal-organic frameworks-modified flexible fiber: preparation and its dopamine sensing application, Chin. Sci. Bull. 66 (2021) 4187–4196.

[19] Z. Zhao, Y. Kong, Z.W. Zhang, G.S. Huang, Y.F. Mei, Atomic layer-deposited nanostructures and their applications in energy storage and sensing, J. Mater. Res. 35 (2020) 701–719.

[20] A.Y.A. Kaassis, S.M. Xu, S. Guan, D.G. Evans, M. Wei, G.R. Williams, Hydroxy double salts loaded with bioactive ions: synthesis, intercalation mechanisms, and functional performance, J. Solid State Chem. 238 (2016) 129–138.

[21] S. Zhu, S. Jiao, Z. Liu, G. Pang, S. Feng, High adsorption capacity for dye removal by CuZn hydroxyl double salts, Environ. Sci. Nano 1 (2014) 172–180.

[22] D. Feng, T.F. Liu, J. Su, M. Bosch, Z. Wei, W. Wan, D. Yuan, Y. Chen, X. Wang, K. Wang, X. Lian, Z. Gu, J. Park, X. Zou, H. Zhou, Stable metal-organic frameworks containing single-molecule traps for enzyme encapsulation, Nat. Commun. 6 (2015) 5979.

[23] J. Park, D. Feng, H.C. Zhou, Dual exchange in PCN-333: a facile strategy to chemically robust mesoporous chromium metal-organic framework with functional groups, J. Am. Chem. Soc. 137 (2015) 11801–11809.

[24] X. Zhang, Q. Liu, X. Shi, A.M. Asiri, X. Sun, An Fe-MOF nanosheet array with superior activity towards the alkaline oxygen evolution reaction, Inorg. Chem. Front. 5 (2018) 1405–1408.

[25] J. Li, L. Liu, Y. Ai, Y. Liu, H. Sun, Q. Liang, Self-polymerized dopamine-decorated Au NPs and coordinated with Fe-MOF as a dual binding sites and dual signal-amplifying electrochemical aptasensor for the detection of CEA, ACS Appl. Mater. Interfaces 12 (2020) 5500–5510.

[26] X. Chen, D. Lau, G. Cao, Y. Tang, C. Wu, In situ synthesis of a sandwich-like graphene@ZIF-67 heterostructure for highly sensitive nonenzymatic glucose sensing in human serums, ACS Appl. Mater. Interfaces 11 (2019) 9374–9384.

[27] Y. Dong, J. Zheng, Tremella-like ZIF-67/rGO as electrode material for hydrogen peroxide and dopamine sensing applications, Sens. Actuators B Chem. 311 (2020) 127918.

[28] C. Duan, J. Zheng, Bimetallic MOF-based enzyme-free sensor for highly sensitive and selective detection of dopamine, J. Electrochem. Soc. 166 (2019) B942–B947.

[29] L. Gaolatlhe, R. Barik, S.C. Ray, K.I. Ozoemena, Voltammetric responses of porous Co3O4 spinels supported on MOF-derived carbons: effects of porous volume on dopamine diffusion processes, J. Electroanal. Chem. 872 (2020) 113863.

[30] T.Y. Huang, C.W. Kung, Y.T. Liao, S.Y. Kao, M. Cheng, T.H. Chang, J. Henzie, H.R. Alamri, Z.A. Alothman, Y. Yamauchi, K.C. Ho, K.C.W. Wu, Enhanced charge collection in MOF-525-PEDOT nanotube composites enable highly sensitive biosensing, Adv. Sci. 4 (2017) 1700261.

[31] J. Li, J. Xia, F. Zhang, Z. Wang, Q. Liu, A novel electrochemical sensor based on copper-based metal-organic framework for the determination of dopamine, J. Chin. Chem. Soc. 65 (2018) 743–749.

[32] B. Ma, H. Guo, M. Wang, L. Li, X. Jia, H. Chen, R. Xue, W. Yang, Electrocatalysis of Cu-MOF/graphene composite and its sensing application for electrochemical simultaneous determination of dopamine and paracetamol, Electroanalysis 31 (2019) 1002–1008.

[33] Z. Qiu, T. Yang, R. Gao, G. Jie, W. Hou, An electrochemical ratiometric sensor based on 2D MOF nanosheet/Au/polyxanthurenic acid composite for detection of dopamine, J. Electroanal. Chem. 835 (2019) 123–129.

[34] G. Yu, J. Xia, F. Zhang, Z. Wang, Hierarchical and hybrid RGO/ZIF-8 nanocomposite as electrochemical sensor for ultrasensitive determination of dopamine, J. Electroanal. Chem. 801 (2017) 496–502.

[35] F. Ma, B. Yang, Z. Zhao, Y. Zhao, R. Pan, D. Wang, Y. Kong, Y.M. Chen, G.S. Huang, J.L. Kong, Y.F. Mei, Sonication-triggered rolling of Janus porous nanomembranes for electrochemical sensing of dopamine and ascorbic acid, ACS Appl. Nano Mater. 3 (2020) 10032–10039.

[36] C. Gong, Y. Shen, J. Chen, Y. Song, S. Chen, Y. Song, Microperoxidase-11@PCN-333 (Al)/three-dimensional macroporous carbon electrode for sensing hydrogen peroxide, Sens. Actuators B Chem. 239 (2017) 890–897.